



Estimating Cotton Water Requirements Using Sentinel-2

Offer Rozenstein^{*1}, Nitai Haymann¹, Gregoriy Kaplan¹, and Josef Tanny^{1,2}

¹Institute of Soil, Water and Environmental Sciences, Agricultural Research Organization, Volcani Center, HaMaccabim Road 68, P.O.B 15159 Rishon LeZion 7528809, Israel

²HIT- Holon Institute of Technology, POB 305, Holon 58102, Israel

**A paper from the Proceedings of the
14th International Conference on Precision Agriculture
June 24 – June 27, 2018
Montreal, Quebec, Canada**

Abstract.

Crop coefficient (K_c)-based estimation of crop water consumption is one of the most commonly used methods for irrigation management. Spectral modeling of K_c is possible due to the high correlations between K_c and the crop phenologic development and spectral reflectance. In this study, cotton evapotranspiration was measured in the field using several methods, including eddy covariance, surface renewal, and heat pulse. K_c was estimated as the ratio between reference evapotranspiration and the measured cotton evapotranspiration. In addition, a time series of Sentinel-2 imagery was processed to produce 22 vegetation indices (VIs) based on the sensor's unique spectral bands. Empirical K_c – VI models were derived and ranked according to their prediction error. In accordance with previous studies, we found a strong correlation between the normalized difference vegetation index (NDVI) and K_c (R² = 0.94), and yet, we also identified other spectral indices that are more strongly correlated to K_c. The indices that were found to be the most suitable for K_c prediction were based on the red and red-edge bands (MTCI, REP, and S2REP). This progress in estimating cotton water consumption using satellite imagery that are available at no cost is a leap forward towards the development of crop irrigation requirements models. Consequently, this work sets the scene for near-real-time irrigation decision support systems.

Keywords. eddy covariance, remote sensing, irrigation, evapotranspiration, spectral modeling.

The authors are solely responsible for the content of this paper, which is not a refereed publication. Citation of this work should state that it is from the Proceedings of the 14th International Conference on Precision Agriculture. EXAMPLE: Lastname, A. B. & Coauthor, C. D. (2018). Title of paper. In Proceedings of the 14th International Conference on Precision Agriculture (unpaginated, online). Monticello, IL: International Society of Precision Agriculture.

1 Introduction

Monitoring the changes of soil and crops status in agricultural fields throughout the growing season is key in increasing the production efficiency. As the crop develops from seedling to a fully mature plant, its transpiration changes accordingly, and so do the crop water requirements. In the early stages of the growing season, the majority of the evapotranspiration is attributed to evaporation from the soil surface. Yet, as the crop develops, the relative contribution of transpiration to the evapotranspiration increases as the vegetation cover increases, and eventually declines with maturity and senescence (Allen et al., 1998). Therefore, information about the crop evapotranspiration (ET_c), which represents the combined water loss due to evaporation from the soil surface and transpiration from the crop, can facilitate better irrigation planning, and ultimately, water use efficiency.

The crop coefficient (K_c) approach for estimating ET_c relies on the estimation of reference evapotranspiration from a hypothetical crop (ET₀) such that $ET_c = K_c \times ET_0$ (Allen et al., 1998). While ET₀ is either calculated based on standard meteorological measurements using the Penman-Monteith Method, or based on pan evaporation measurements, K_c is derived experimentally per crop and soil type and thus separates the climatic demand from the plant response (Duchemin et al., 2006; Kumar et al., 2012).

The United Nations' Food and Agricultural Organization (FAO) has provided details on the development and use of K_c values for different crops in different parts of the world (Allen et al., 1998). However, K_c has been shown to vary between sites and between seasons (Kumar et al., 2015). Additionally, in cases of atypical crop development and water-use patterns caused by weather anomalies, adopting the FAO-recommended K_c values often results with imprecise ET_c estimations (Hunsaker et al., 2003). As a result, local adaptations to the FAO-recommended K_c values are implemented to form local K_c tables, but even these sometimes fail to capture deviations from standard conditions due to specific fertilization, variations in crop planting density, and stress factors such as pests (Kumar et al., 2015). In addition, the spatial variation in ET_c due to spatial heterogeneity in soil characteristics such as water holding capacity and nutrients availability is not reflected in standard K_c tables. Accordingly, in the absence of reliable, real-time information about ET_c, there is a need for better K_c estimates.

One approach to address this need is by using satellite remote sensing imagery. This technology is attractive for modeling K_c since it provides a synoptic coverage at fixed time intervals, and can therefore monitor changes over time (Rozenstein & Adamowski, 2017a; Rozenstein & Adamowski, 2017b). Moreover, spectral vegetation indices (VIs) derived from remote sensing imagery are highly correlated with crop characteristics including biomass, Leaf Area Index (LAI), plant height, and yield (Thenkabail et al., 2000; Duchemin et al., 2006; Park et al., 2017). Similarly, VIs can serve as near-real-time surrogates for K_c since they depict a similar temporal pattern (Jackson et al., 1980; Kamble et al., 2013). Although the commonly used Normalized Difference Vegetation Index (NDVI) is known to saturate at LAI>3 (Asner et al., 2004), there is a similarity between the NDVI–LAI and K_c–LAI curves, suggesting that both plant transpiration and light absorption increase roughly at the same rate at the beginning of the season, and then saturates (Duchemin et al., 2006). Since both K_c and NDVI saturate at about the same time, the loss of accuracy in the estimate of high LAI due to NDVI saturation will have little impact on the accuracy of transpiration estimates, and in addition, the relationship between NDVI and K_c is linear (Duchemin et al., 2006).

In order to model K_c using VIs, most previous studies employed ET_c field measurements using lysimeters or eddy covariance systems (Kamble et al., 2013; Er-Raki et al., 2013; Park et al., 2017; Jin et al., 2017). In other studies, field measurements were not conducted to estimate K_c, but some adaptations from FAO recommendations were made for the local meteorological conditions (e.g. Ray & Dadhwal, 2001; Farg et al., 2012). Hence, ground truth (i.e. evapotranspiration measurements in the field) can be used as training data for K_c prediction

models based on remote sensing VIs.

The basic limitation of satellite remote sensing application for irrigation management is the compromise between the sensor's revisit time and spatial resolution. Sensors with a short revisit time such as the moderate-resolution imaging spectroradiometer (MODIS) that provides daily coverage are characterized by a coarse spatial resolution (>250 m), while sensors with medium spatial resolution such as the Landsat series are characterized by longer revisit times (16 days). Cloudy conditions further reduce the temporal resolution for all optical sensors, thus posing another limitation on operational applications. Irrigation management decisions for field crop should ideally be based on a dense time series of imagery that are fine grained enough to distinguish between field plots. Commercial high spatial resolution satellite sensors such as the Worldview series, RapidEye, GeoEye, QuickBird, and Ikonos, are not routinely employed for crop monitoring because their imagery are not public domain and come at a significant cost, rendering them too expensive for most operational agricultural applications. Therefore, in spite of established K_c – VIs models, the limited availability of imagery with suitable temporal and spatial resolutions at no or low cost hindered the development of worldwide operational systems to estimate K_c from VIs, and prevented wide remote sensing application for near-real-time irrigation decisions.

The successful recent deployment of the two Sentinel-2 satellites creates a unique opportunity for operational K_c estimates. Sentinel-2 multispectral spaceborne imagery with a 5-day revisit time (obtained by the combination of Sentinel-2A and Sentinel-2B data) can potentially create a dense K_c time series at 10 m spatial resolution, which would allow the application of this technique even for small fields (Frampton et al., 2013). It was recently demonstrated that a combination of Landsat-8 (30 m, 16-day revisit), Deimos-1 (22 m, 3-day revisit) and the SPOT4-Take5 experiment (20 m, 5-day revisit) can produce an observation frequency similar to Sentinel-2A and Sentinel-2B, albeit at a lower spatial resolution (Battude et al., 2017). Additionally, most of the VIs that have been previously employed for this task were based on bands covering the visible and near infrared (NIR) spectral regions, since these bands were traditionally available for sensors like Landsat and SPOT (Thenkabail et al., 2000; Battude et al., 2017). Sentinel-2 also features those traditional bands, alongside additional bands in the red-edge region that is very sensitive to crop characteristics such as leaf area index (Viña et al., 2011; Frampton et al., 2013; Nguy-Robertson et al., 2014).

The above literature review suggests that Sentinel-2 imagery offers an acceptable compromise between the revisit time and spatial resolution, with increased spectral abilities for vegetation monitoring compared to previous public domain spaceborne imagery. Hence, the overarching aim of this research was to develop methodology to estimate cotton water consumption based on Sentinel-2 imagery. The key objectives of this study were to (1) estimate daily ET_c experimentally in the field, and (2) develop empirical models that link ET_c with remotely sensed spectral indices from Sentinel-2.

2 Material and Methods

2.1 Study Site

The measurements took place during the summer of 2016 in a cotton field near Gedera, in the Shfela region in Israel (Fig. 1). This field was chosen because it was relatively flat, and large enough to contain most of the flux footprint measured by the eddy-covariance system (described in section 2.2.1). Field had a trapeze shape, with a mean length of 780 m and mean width of 540 m (the long dimension was oriented east-west, see Fig. 1 right). Cotton, cv. Pima, was sowed in the soil in east-west rows on March 10, 2016, and was drip-fertigated. Precipitation and irrigation during the growing season are plotted in Fig. 2. The irrigation was stopped on September 5, 2016, and the cotton was harvested on October 5, 2016.

Field measurements were conducted during July and August 2016. The local summer climate is rainless, with little variation from day to day. According to data supplied by the Agro-Meteorology

unit of the Israel Ministry of Agriculture and Rural Development from the Revadim meteorological station, about 4 km south of the experiment location, between January 2008 and December 2016 the annual average number of rainy days, i.e., rainfall ≥ 1 mm, was 51, with an annual average rainfall of 469 mm. There was no rainfall during the summer months – June through August. The annual average and the growing season average (March-September) of meteorological data from 2008 – 2016 were: relative humidity 64.6 and 64.4%, respectively; relative humidity at 12:00 GMT – 49.9 and 47.7%, respectively; mean daily air temperature – 20.2 and 22.8°C, respectively; mean daily minimum air temperature – 15.4 and 17.5°C, respectively; and corresponding mean daily maximum temperature – 25.5 and 28.3°C, respectively.

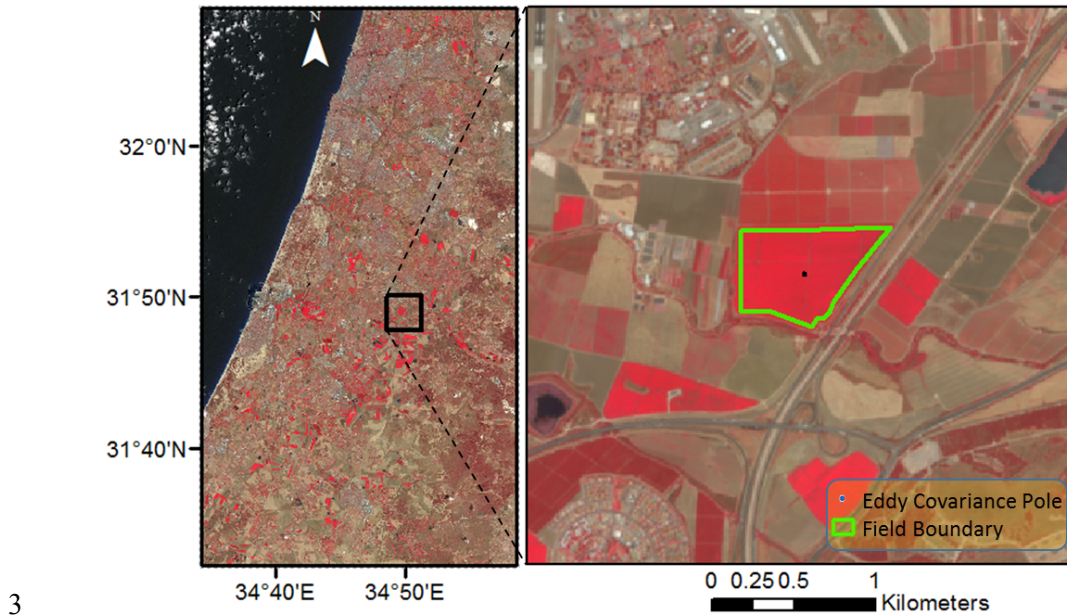


Fig. 1. Left: Sentinel-2A false color regional image (RGB = bands 8,4,3) acquired on 25 July 2016. The black square represents the footprint of the image on the right, showing a blow-up of the area around the study site.

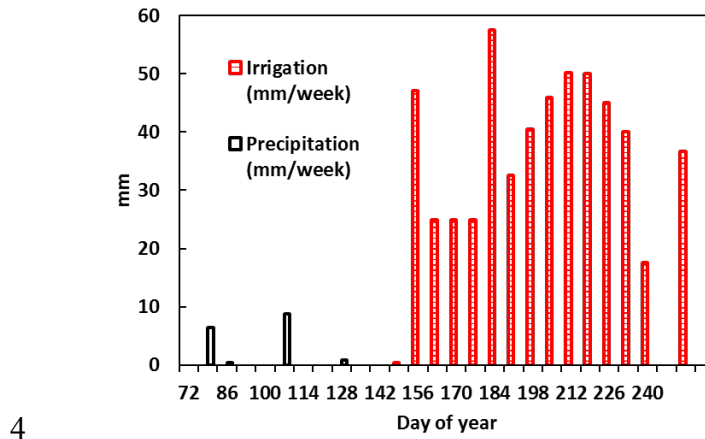


Fig 2. Precipitation (measured at the Revadim meteorological station, operated by the Agro-Meteorology unit of the Israel Ministry of Agriculture and Rural Development, 4 km south of the field) and irrigation during the cotton growing season (irrigation data provided by the grower).

4.1 Agro-Meteorological Measurements

4.1.1 Reference Evapotranspiration – ET_0

The Agro-Meteorology unit of the Israel Ministry of Agriculture and Rural Development regularly estimates the reference evapotranspiration (ET_0) at selected locations across Israel. In this study, ET_0 was calculated according to the Penman-Monteith method (Allen et al., 1998) based *Proceedings of the 14th International Conference on Precision Agriculture June 24 – June 27, 2018, Montreal, Quebec, Canada*

on meteorological measurements of temperature, relative humidity, wind speed and solar irradiance at the Revadim meteorological station located about 4 km south of the study site. This public-domain data is available for download from: <http://www.meteo.co.il/>.

4.1.2 Eddy Covariance (EC)

Direct measurements of ET_c (actual crop evapotranspiration) were done by an eddy covariance system that measured latent and sensible heat fluxes. An eddy covariance (EC) system was deployed at a height of 3.65 m on a tower located within the field (Fig. 1b) at a position that allowed a fetch of about 400 m for the prevailing northwesterly wind. The system consisted of a three-axis ultrasonic anemometer (Model CSAT3; Campbell Scientific, Logan, UT, USA) that measured the wind speed vector and sonic temperature, and an Infra-Red Gas Analyzer, IRGA (Model LI-7500; LI-COR, Lincoln, NE, USA) that measured water-vapor concentration. To minimize wind distortion effects, the CSAT3 anemometer head was oriented towards the approximate direction of the predominant wind. Raw signals from the EC system were sampled at 20 Hz. Signals were recorded on a CR3000 data logger (Campbell Scientific, Logan, UT, USA) and later processed by the EddyPro software (LI-COR, Lincoln, NE, USA) to generate the flux data. The EddyPro software estimated the distance of the 90% flux footprint of each 30-min data point, later used to select the analysis polygon (see section 2.3.1). EC evapotranspiration data were used for DOYs 180-189, 195-206, 211-213, 215-217, 221-228, 243-244, 249-251, 256-257.

4.1.3 Surface Energy Balance

Additional measurements facilitated energy-balance closure analysis. Net radiation (R_n) was measured with a net radiometer (Q*7.1; REBS, Seattle, WA, USA) installed at 3.65 m height, on the same pole of the EC system. Air temperature and relative humidity were measured by a sensor (HMP45, Campbell Sci., Logan, UT, USA) positioned at a height of 3.5 m within a ventilated radiation shield. Soil heat flux (G) was measured with four soil heat flux plates (HFT-3.1; REBS, Seattle, WA, USA) installed at a depth of 0.08 m within the soil and two thermocouples type T (copper-constantan) that were installed in the soil layer above each plate at depths of 0.02 and 0.06 m (total of 8 thermocouples). The calculation of soil heat flux and storage was done similarly to the procedure described by Rosa et al. (2013) and Tanny et al. (2006). Thirty-minute averages of measured variables (net radiation, soil heat flux, and soil temperatures) were recorded on a CR23X data logger (Campbell Scientific, Logan, UT, USA). All the equipment was powered by car batteries that were charged during the day by solar panels.

4.1.4 Surface Renewal (SR)

The surface renewal method estimates H, the sensible heat flux, from high frequency, single point temperature measurement, and then extracts the evapotranspiration as a residual of the energy balance closure (Paw U et al., 1995). The method proved reliable for cotton evapotranspiration measurements (Rosa & Tanny, 2015). In the present field experiment, a miniature thermocouple type T, 50 µm in diameter (COCO-002, Omega Eng., UK), was installed at 1.5 m height on the same mast of the EC system. The sensor measured air temperature at 10 Hz and raw data was recorded on a CR3000 data logger (Campbell Scientific, Logan, UT, USA). Sensible heat flux calculated by SR data analysis (Spano et al., 1997) was calibrated against direct EC measurements and the calibration coefficient was utilized during periods when EC data were unavailable. SR evapotranspiration data were used for DOYs 207-210, and 218-220.

4.1.5 Heat Pulse

Sap flow measurements were conducted using the heat-pulse technique. Sensors were installed in 12 cotton plants about 200 m west of the position of the EC mast. In the present analysis, we assume that for the high-density cotton field, soil evaporation is negligible; hence, evapotranspiration and transpiration are equal. SF transpiration data were used for DOYs 235-242, 245-248, 252-255, 258-261.

4.1.6 Derivation of the crop-coefficient (K_c)

The crop coefficient was derived according to Allen et al. (1998):

$$K_c = \frac{ET_c}{ET_o} \quad (1)$$

where ET_c is the crop evapotranspiration as measured by eddy covariance, surface renewal or sap flow method. Our gold standard was the eddy covariance measurement, however, at times the eddy covariance system failed, creating a gap in the time series. During the days that the eddy covariance system did not provide data, ET_c was estimated using either the surface renewal or the sap flow measurements.

4.2 Satellite Measurements

4.2.1 Pre-Processing

A total of seven relatively cloud free Sentinel-2A images acquired during the cotton-growing season were analyzed in this study, including five images that coincide with our agro-meteorological measurements. The images were atmospherically corrected using sen2cor (Louis et al., 2016) and processed using the Sentinel-2 Toolbox, an extension of SeNtinel Application Platform (SNAP) (Gascon & Ramoino, 2017).

In order to select the pixels for analysis, a polygon defining the borders of the cotton field was demarked. Furthermore, the point density of the 90% flux footprint of eddy-covariance measurements taken between 7 am and 6 pm was calculated. A threshold of 0.018 points per m² was selected to create a second polygon representing the area from which most of the flux measured by the eddy-covariance system was originated. Cloud and cloud shadow masks were generated for the five Sentinel-2A images that coincide with the agro-meteorological measurements. The intersection between the field borders, the area that represents the flux footprint, and the cloud masks defined the polygon of the analysis area (Fig. 3).

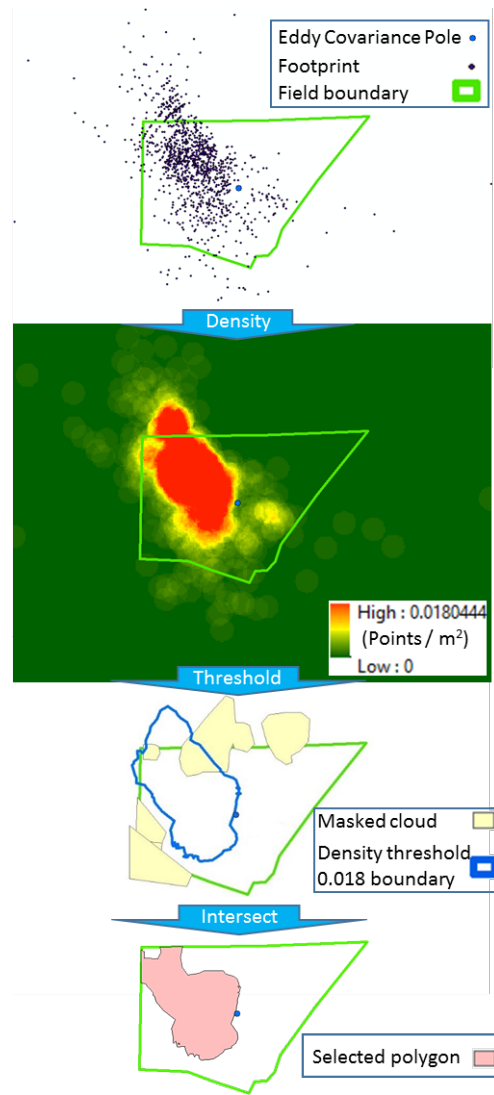


Fig. 3: The process of determining the analysis area by thresholding the density map of eddy covariance footprint distribution and intersecting with areas masked by clouds on some images, and by the field boundaries.

4.2.2 Spectral Indices

We applied the 22 vegetation indices included in SNAP to all of the images throughout the growing season (Table 1).

Table 1: Vegetation indices and their application using Sentinel-2 bands.

Index Name	Formula	Sentinel-2 Band Assignments	Reference
MERIS terrestrial chlorophyll index (MTCI)	$\frac{(NIR - RE)}{(RE - RED)}$	$\frac{(B6 - B5)}{(B5 - B4)}$	(Dash & Curran, 2007)
Red Edge In-flection Point (REIP)	$700 + 40 * \frac{R670+R780 - R700}{R740 - R700}$	$700 + 40 * \frac{B4 + B7 - B5}{B6 - B5}$	(Guyot et al., 1988)
Atmospherically Resistant Vegetation Index (ARVI)	$\frac{(NIR - 2 * RED - BLUE)}{(NIR + 2 * RED - BLUE)}$	$\frac{(B08 - 2 * B04 - B02)}{(B08 + 2 * B04 - B02)}$	(Kaufman & Tanre, 1992)
Soil Adjusted Vegetation Index	$\frac{(NIR - RED)}{(NIR + RED + L)} * (1 + L)$	$\frac{(B08 - B04)}{(B08 + B04 + 0.5)} * (1.5)$	(Huete, 1988)

(SAVI)			
Modified Soil Adjusted Vegetation Index 2 (MSAVI2)	$\frac{([2 * NIR + 1 - \sqrt{((2 * NIR + 1)^2 - 8 * (NIR - RED))}])/2}$	$\frac{([2 * B08 + 1 - \sqrt{((2 * B08 + 1)^2 - 8 * (B08 - B04))}])/2}$	(Qi et al., 1994)
Infrared Percentage Vegetation Index (IPVI)	$\frac{NIR}{(NIR + RED)}$	$\frac{B8}{(B8 + B4)}$	(Crippen, 1990)
Normalized Difference Vegetation Index (NDVI)	$\frac{(NIR - RED)}{(NIR + RED)}$	$\frac{(B8 - B4)}{(B8 + B4)}$	(Tucker, 1979)
Modified Soil Adjusted Vegetation Index (MSAVI)	$\frac{(NIR - RED) * (1 + L)}{(NIR + RED + L)}$ where: $L = 1 - \frac{2 * s * (NIR - RED) * (NIR - s * RED)}{(NIR + RED)}$	$\frac{(B8 - B4) * (1 + L)}{(B8 + B4 + L)}$ where: $L = 1 - 2 * s * NDVI * WDWI$ and $s = 0.5$	(Qi et al., 1994)
Transformed Normalized Difference Vegetation Index (TNDVI)	$\sqrt{\frac{(NIR - RED)}{(NIR + RED)} + 0.5}$	$\sqrt{\frac{(B8 - B4)}{(B8 + B4)} + 0.5}$	(Deering, 1975)
Green Normalized Difference Vegetation Index (GNDVI)	$\frac{(NIR - GREEN)}{(NIR + GREEN)}$	$\frac{(B7 - B3)}{(B7 + B3)}$	(Gitelson & Merzlyak, 1998)
Inverted Red-Edge Chlorophyll Index (IRECI)	$\frac{(NIR - RED)}{(RE1/RE2)}$	$\frac{(B7 - B4)}{(B5 / B6)}$	(Frampton et al., 2013)
Global Environmental Monitoring Index (GEMI)	$\frac{\hat{\eta} * (1 - 0.25 * \hat{\eta}) - \frac{[(RED - 0.125)}{(1 - RED)]}{(NIR + RED + 0.5)}}$ where $\hat{\eta} = \frac{[2 * (NIR^2 - RED^2) + 1.5 * NIR + 0.5 * RED]}{(NIR + RED + 0.5)}$	$\frac{\hat{\eta} * (1 - 0.25 * \hat{\eta}) - \frac{(B4 - 0.125)}{(1 - B4)}}{(B8A + B4 + 0.5)}$ where $\hat{\eta} = \frac{[2 * (B8A^2 - B4^2) + 1.5 * B8A + 0.5 * B4]}{(B8A + B4 + 0.5)}$	(Pinty & Verstraete, 1992)
Normalized Difference Index 45 (NDI45)	$\frac{(NIR - RED)}{(NIR + RED)}$	$\frac{(B5 - B4)}{(B5 + B4)}$	(Delegido et al., 2011)
Perpendicular Vegetation Index (PVI)	$\sqrt{(\rho G_{ir,s} - P_{ir})^2 + (\rho G_{r,s} - P_r)^2}$	$\sin(a) * B8 - \cos(a) * B4$ where $a = 45^\circ$	(Richardson & Wiegand, 1977)
Difference Vegetation Index (DVI)	$NIR - RED$	$B8 - B4$	(Tucker, 1979)
Pigment Specific Simple Ratio (PSSRa)	$\frac{RE}{RED}$	$\frac{B7}{B4}$	(Blackburn, 1998)
Ratio Vegetation Index (RVI)	$\frac{NIR}{RED}$	$\frac{B8}{B4}$	(Pearson & Miller, 1972)
Weighted Difference Vegetation Index (WDVI)	$NIR - S * RED$	$B8 - S * B4$ Where $S = 0.5$	(Clevers, 1989)
Transformed Soil Adjusted Vegetation Index (TSAVI)	$\frac{([A * (NIR - A * RED - B)])}{(RED - (A * B) + X(1 + A^2))}$	$\frac{s * ((B8 - s * B4 - a))}{((a * B8 + B4 - a * s + X * (1 + s * s)))}$ Where $a = 0.5$; $s = 0.5$; $X = 0.08$	(Baret et al., 1989)
Sentinel-2 Red-Edge Position (S2REP)	$705 + 35 * \frac{(p783 + p665)}{p740 - p705} - p705$	$705 + 35 * \frac{(B4 + B7)}{(B6 - B5)} - B5$	(Frampton et al., 2013)
Modified Chlorophyll Absorption Ratio Index (MCARI)	$\left[\frac{(RE - RED)}{0.2 * (RE - GREEN)} \right] * RE / RED$	$[(B5 - B4) - 0.2 * (B5 - B3)] * \frac{B5}{B4}$	(Daughtry et al., 2000)
Enhanced Vegetation Index (EVI)	$(2.5 * (NIR - RED)) / ((NIR + 6 * RED - 7.5 * BLUE + 1))$	$(2.5 * (B8 - B4)) / ((B8 + 6 * B4 - 7.5 * B2 + 1))$	(Huete et al., 2002)

Linear regression models were developed for the time series of field measured Kc and the time series of each spectral index. R2 and Root Mean Square Error (RMSE) values were calculated

for every model. The K_c -NDVI model developed in this study was compared to other similar models from the literature that were developed for cotton (Montgomery et al., 2015) and with a general field crop model (Kamble et al., 2013). In addition, the field measured K_c values, and the estimates of K_c -NDVI models were compared with the recommended K_c for cotton in this region that is provided by the Israeli Extension Service.

5 Results

Energy balance closure was analyzed in order to verify the eddy covariance flux measurements (Fig. 4). The 0.99 slope, which represents a nearly perfect closure, and high coefficient of determination ($R^2 = 0.92$) between $LE+H$ and $Rn-G$ demonstrate that the eddy covariance fluxes were reliable in determining the crop evapotranspiration.

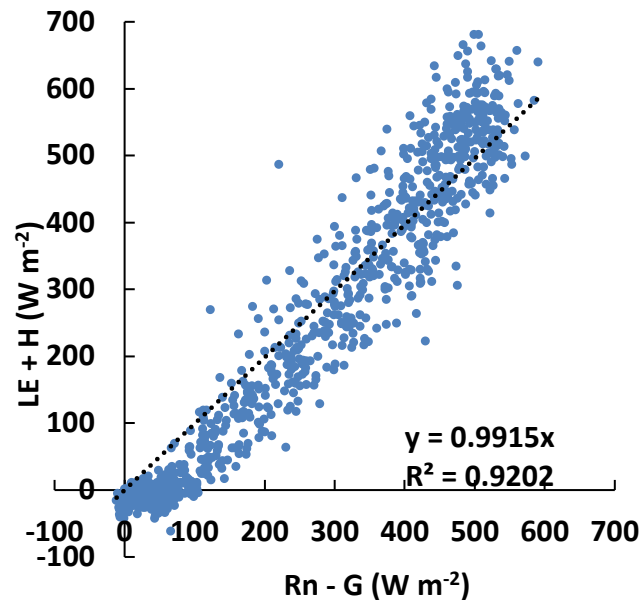


Fig. 4. Energy balance closure: the relation between the energy consumed by the canopy ($LE+H$) and the available energy ($Rn-G$), where LE and H are latent and sensible heat fluxes respectively, Rn is net radiation, and G is soil heat flux.

The mid-late season K_c demonstrates a very similar temporal pattern to NDVI (Fig. 5). Linear regression models between each of the 22 VIs and K_c were derived, and most of these models show high correlation between K_c and the Sentinel-2 VIs (Table 2). These results strengthen the case for using VIs as surrogates for K_c . The three best models (ranked according to RMSE) are based on VI composed of bands covering the red and red-edge spectral bands (MTCI, REP, S2REP). Models based on five more indices (ARVI, SAVI, MSAVI2, IPVI, MSAVI) performed better in predicting K_c than the popularly used NDVI. However, despite its hinge on red and red-edge bands, IRECI, PSSRa, and MCARI did not perform better than NDVI for predicting K_c . Comparison of the NDVI model developed in this study with models from the literature (Kamble et al., 2013; Montgomery et al., 2015) shows an increase of about one order of magnitude in RMSE in the other models (Fig. 6). Even though the Kamble et al. model is a general model developed for multiple field crops, and the Montgomery et al. model was developed for cotton, both have similar prediction errors and they both over estimate K_c by about 0.2 compared to our field measurements, and by 0.04 to 0.36 compared to the standard recommendation by the Israeli Extension Service (Fig. 7). The Israeli Extension Service recommendation was higher than the measured K_c for most of the time, except for one point at the end of the season (Fig. 7). Therefore, following the standard Israeli Extension Service K_c table recommendations, the

Montgomery et al. (2015) model or the Kamble et al. (2013) model would lead to excess irrigation.

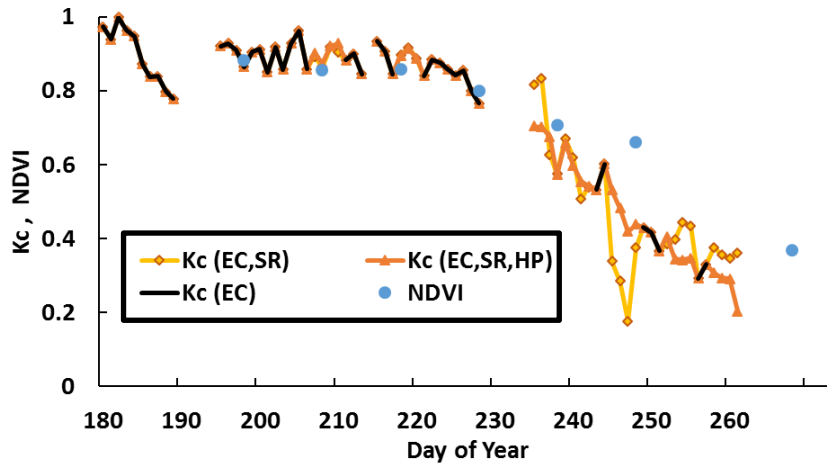


Fig. 5: The temporal trajectory of NDVI from seven Sentinel-2 images and Kc based on Eddy Covariance (EC), EC and Surface Renewal (EC, SR), and EC, SR and Heat-Pulse (EC, SR, HP) methods. The combination of all three methods (EC, SR, HP) produced the most continuous time series, and therefore it was used to model Kc.

Table 2: The R² and RMSE of Linear Kc – Vegetation Index regression models, ranked according to RMSE.

Index	R ²	RMSE
MTCI	0.9915	0.0079
REIP	0.9942	0.0125
S2REP	0.9942	0.0134
ARVI	0.9582	0.0175
SAVI	0.9576	0.0176
MSAVI2	0.952	0.0188
IPVI	0.9493	0.0193
MSAVI	0.9492	0.0193
NDVI	0.9491	0.0193
TNDVI	0.949	0.0193
GNDVI	0.9484	0.0194
IRECI	0.9408	0.0208
GEMI	0.9372	0.0214
EVI	0.9206	0.0241
NDI45	0.91	0.0257

PVI	0.896	0.0276
DVI	0.8959	0.0276
PSSRa	0.8902	0.0284
RVI	0.8843	0.0291
WDVI	0.8178	0.0365
TSAVI	0.7673	0.0413
MCARI	0.3199	0.0706
NDVI (Kamble et al.)		0.1969
NDVI (Montgomery et al.)		0.2118

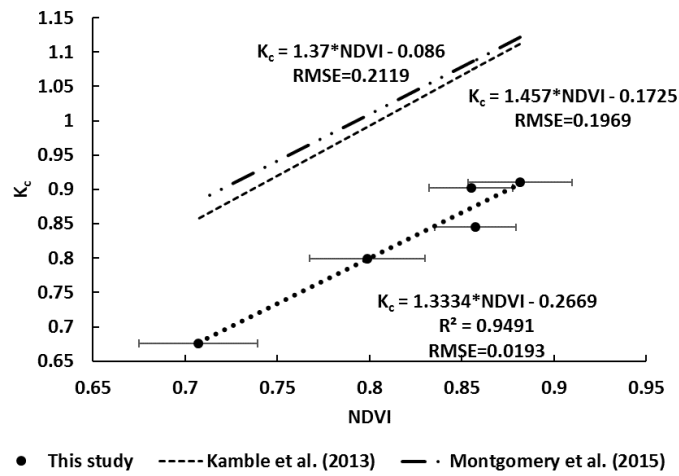


Fig. 6: Comparison of K_c – NDVI regression models (Kamble et al., 2013; Montgomery et al., 2015) with the model developed in this study.

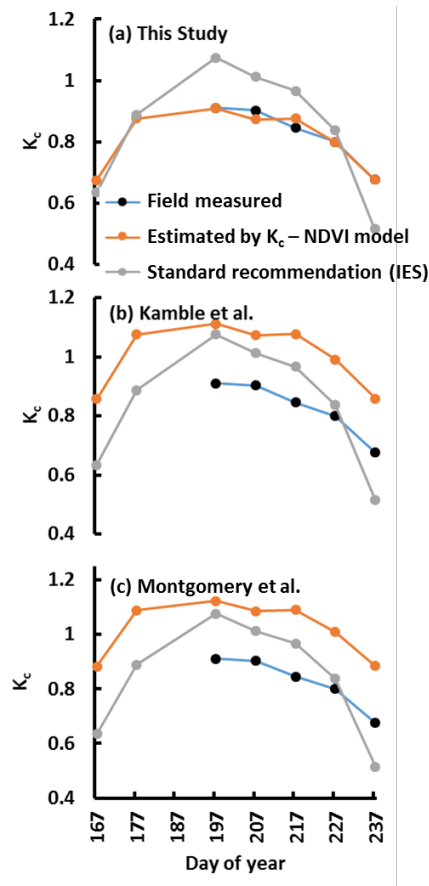


Fig. 7: Field measured K_c for cotton in this study, and the standard K_c recommendation by the Israeli Extension Service (IES) for cotton growers in this region compared to estimates according to three K_c - NDVI models: (a) The model developed in this study; (b) Kamble et al. (2013); (c) Montgomery et al. (2015).

6 Discussion

Our results suggest that most VIs that are based on Sentinel-2 bands are suitable predictors for cotton K_c , and that those based on the red and red-edge spectral bands (MTCI, REP, and S2REP) are the best ones. In contrast to previous studies that mostly used VIs based on red and NIR bands (NDVI, SAVI, etc.) to model K_c , our study suggests that we can now develop more accurate models using the new Sentinel-2 compared to previous sensors (e.g. Landsat). This result is in agreement with previous studies that showed that red edge based VIs correlate better with chlorophyll content and LAI (Viña et al., 2011; Frampton et al., 2013; Nguy-Robertson et al., 2014). Therefore, it is not surprising that these indices exhibited the highest correlations with our field measured K_c .

Our K_c estimation models for cotton were different from the standard K_c recommendations by IES, and different from literature K_c estimates based on VI - NDVI models. This suggests that K_c - VI models are specific to local conditions and accordingly, their development and application should be crop and region specific to achieve the best K_c estimation. Therefore, published K_c - VI models should be very carefully adapted for use in different settings than the ones they were developed in.

Our field measurements were carried out during the mid-late stages of the growing season. This can explain the extremely high correlation we found for some K_c - VI models. Peaks in evaporation following irrigation or rain events, and the sensitivity of some VIs to the soil top-layer wetness, usually result with lower K_c - VI correlations at the beginning of the season when the vegetation is sparse, and higher at the end of the season since the vegetation, even senescent, is limiting soil evaporation (e.g. Duchemin et al., 2006). Thus, the models presented in this paper still

require further testing and possibly adaptations to extend their application to the entire growing season. In a future study, we intend to perform eddy covariance measurements throughout the growing season to validate and improve the models developed in this study. In addition, Kc estimates are based on an assumption that the commercial field where the experiment took place was well watered, which is the common practice of cotton growers in this region, and indeed, the irrigation (Fig. 2) was consistently higher than the field measurements of crop evapotranspiration. The reason for this assumption is that Kc –VI models based on optical remote sensing data do not allow estimating actual evapotranspiration but provide a maximal value that would be observed if water were readily available in the soil (Duchemin et al., 2006). Therefore, at this stage, the present remote-sensing based Kc estimates may prove inaccurate for a water stressed crop.

While our study was conducted during the summer of 2016, when data from only Sentinel-2A was available, nowadays Sentinel-2B is already in orbit and operational. Thus, for future studies, the technique demonstrated in this paper can be applied at double the temporal resolution. Even with only Sentinel-2A at our disposal, we were able to obtain seven clear images during the mid-late growing season. Unlike other studies that interpolated the VI time series between satellite image acquisition to compensate for the low temporal resolution of imagery (e.g. Duchemin et al., 2006), we did not perform any interpolation and relied solely on actual Sentinel-2 measurements to ensure that the model is calibrated using actual field measurements. Since our field measurements were not entirely continuous, we did not measure ETc on every day, and as a result, our models are based on only five out of the seven available images.

Together, Sentinel-2A and Sentinel-2B offer better revisit time (5 days vs. 16 days), and better spatial resolution (10 m vs. 30 m), compared to Landsat-8. However, Landsat-8's Thermal Infrared Sensor (TIRS) does provide information on the land surface temperature (Rozenstein et al., 2014) that is not available from Sentinel-2, and therefore, in the context of modeling evapotranspiration, Landsat-8 is still extremely valuable (Senay et al., 2016). Moreover, the Harmonized Landsat/Sentinel-2 data set that is currently under development (Masek et al., 2015; Flood, 2017) can further improve the revisit time at the expense of spatial resolution (the harmonized product resolution is 30 m) and the loss of red edge based indices since Landsat-8 Operational Land Imager (OLI) does not include red-edge bands.

7 Conclusion

Sentinel-2 is superior to older generations of public domain satellite data in terms of spatial, temporal and spectral resolutions. This allows, for the first time, to estimate Kc, an important parameter for irrigation management, at a high frequency that can support irrigation decisions, at a fine spatial resolution of 10 m that well captures within field variability, and at higher accuracy than before, owing to the sensor's unique spectral bands that cover the red-edge region.

Acknowledgements

This study was partially supported by an ARO Start-Up Grant held by Offer Rozenstein. Gregoriy Kaplan was supported by an absorption grant for new immigrant scientists provided by the Israeli Ministry of Immigrant Absorption. Dr. Shabtai Cohen is thanked for providing the equipment to perform the sap flow measurements, and for reviewing an early version of the manuscript. We thank Mr. Victor Lukyanov and Mr. Ori Achiman for technical support with the field measurements. The field measurements were funded by the Chief Scientist of the Ministry of Agriculture, Israel, under grant number 304-0505.

References

- Allen, R.G., Pereira, L.S., Raes, D., & Smith, M. (1998). Crop evapotranspiration-Guidelines for computing crop water requirements-FAO Irrigation and drainage paper 56. FAO, Rome, 300, D05109.
- Asner, G.P., Nepstad, D., Cardinot, G., & Ray, D. (2004). Drought stress and carbon uptake in an Amazon forest measured with spaceborne imaging spectroscopy. *Proceedings of the National Academy of Sciences of the United States of America*, 101, 6039-6044.

- Baret, F., Guyot, G., & Major, D.J. (1989). Crop biomass evaluation using radiometric measurements. *Photogrammetria*, 43, 241-256.
- Battude, M., Al Bitar, A., Brut, A., Tallec, T., Huc, M., Cros, J., et al. (2017). Modeling water needs and total irrigation depths of maize crop in the south west of France using high spatial and temporal resolution satellite imagery. *Agricultural Water Management*, 189, 123-136.
- Blackburn, G.A. (1998). Quantifying Chlorophylls and Carotenoids at Leaf and Canopy Scales. *Remote Sensing of Environment*, 66, 273-285.
- Clevers, J.G.P.W. (1989). Application of a weighted infrared-red vegetation index for estimating leaf Area Index by Correcting for Soil Moisture. *Remote Sensing of Environment*, 29, 25-37.
- Crippen, R.E. (1990). Calculating the vegetation index faster. *Remote Sensing of Environment*, 34, 71-73.
- Dash, J., & Curran, P.J. (2007). Evaluation of the MERIS terrestrial chlorophyll index (MTCI). *Advances in Space Research*, 39, 100-104.
- Daughtry, C.S.T., Walthall, C.L., Kim, M.S., de Colstoun, E.B., & McMurtrey, J.E. (2000). Estimating Corn Leaf Chlorophyll Concentration from Leaf and Canopy Reflectance. *Remote Sensing of Environment*, 74, 229-239.
- Deering, D. (1975). Measuring forage production of grazing units from Landsat MSS data. *Proceedings of 10th international symposium on remote sensing of environment*, 1975, 1169-1178.
- Delegido, J., Verrelst, J., Alonso, L., & Moreno, J. (2011). Evaluation of sentinel-2 red-edge bands for empirical estimation of green LAI and chlorophyll content. *Sensors*, 11, 7063-7081.
- Duchemin, B., Hadria, R., Erraki, S., Boulet, G., Maisongrande, P., Chehbouni, A., et al. (2006). Monitoring wheat phenology and irrigation in Central Morocco: On the use of relationships between evapotranspiration, crops coefficients, leaf area index and remotely-sensed vegetation indices. *Agricultural Water Management*, 79, 1-27.
- Er-Raki, S., Rodriguez, J.C., Garatuza-Payan, J., Watts, C.J., & Chehbouni, A. (2013). Determination of crop evapotranspiration of table grapes in a semi-arid region of Northwest Mexico using multi-spectral vegetation index. *Agricultural Water Management*, 122, 12-19.
- Farg, E., Arafat, S.M., Abd El-Wahed, M.S., & EL-Gindy, A.M. (2012). Estimation of Evapotranspiration E_{Tc} and Crop Coefficient K_c of Wheat, in south Nile Delta of Egypt Using integrated FAO-56 approach and remote sensing data. *The Egyptian Journal of Remote Sensing and Space Science*, 15, 83-89.
- Flood, N. (2017). Comparing Sentinel-2A and Landsat 7 and 8 Using Surface Reflectance over Australia. *Remote Sensing*, 9, 659.
- Frampton, W.J., Dash, J., Watmough, G., & Milton, E.J. (2013). Evaluating the capabilities of Sentinel-2 for quantitative estimation of biophysical variables in vegetation. *ISPRS Journal of Photogrammetry and Remote Sensing*, 82, 83-92.
- Gascon, F., & Ramoino, F. (2017). Sentinel-2 data exploitation with ESA's Sentinel-2 Toolbox. *EGU General Assembly Conference Abstracts*, 19, 19548.
- Gitelson, A.A., & Merzlyak, M.N. (1998). Remote sensing of chlorophyll concentration in higher plant leaves. *Advances in Space Research*, 22, 689-692.
- Guyot, G., Baret, F., & Major, D. (1988). High spectral resolution: Determination of spectral shifts between the red and the near infrared. *International Archives of Photogrammetry and Remote Sensing*, 11.
- Huete, A., Didan, K., Miura, T., Rodriguez, E.P., Gao, X., & Ferreira, L.G. (2002). Overview of the radiometric and biophysical performance of the MODIS vegetation indices. *Remote Sensing of Environment*, 83, 195-213.
- Huete, A.R. (1988). A soil-adjusted vegetation index (SAVI). *Remote Sensing of Environment*, 25, 295-309.
- Hunsaker, D.J., Pinter, P.J., Barnes, E.M., & Kimball, B.A. (2003). Estimating cotton evapotranspiration crop coefficients with a multispectral vegetation index. *Irrigation Science*, 22, 95-104.
- Jackson, R., Idao, S., Reginato, R., & Pinter, P. (1980). Remotely sensed crop temperatures and reflectances as inputs to irrigation scheduling. *Irrigation and drainage special conference proceedings*, 390-397.
- Jin, X., Yang, G., Xue, X., Xu, X., Li, Z., & Feng, H. (2017). Validation of two Huanjing-1A/B satellite-based FAO-56 models for estimating winter wheat crop evapotranspiration during mid-season. *Agricultural Water Management*, 189, 27-38.
- Kamble, B., Kilic, A., & Hubbard, K. (2013). Estimating crop coefficients using remote sensing-based vegetation index. *Remote Sensing*, 5, 1588-1602.
- Kaufman, Y.J., & Tanre, D. (1992). Atmospherically resistant vegetation index (ARVI) for EOS-MODIS. *Geoscience and Remote Sensing*, 30, 261-270.
- Kumar, R., Jat, M., & Shankar, V. (2012). Methods to estimate irrigated reference crop evapotranspiration—a review. *Water Science and Technology*, 66, 525-535.
- Kumar, V., Udeigwe, T.K., Clawson, E.L., Rohli, R.V., & Miller, D.K. (2015). Crop water use and stage-specific crop coefficients for irrigated cotton in the mid-south, United States. *Agricultural Water Management*, 156, 63-69.
- Louis, J., Debaecker, V., Pflug, B., Main-Knorn, M., Bieniarz, J., Mueller-Wilm, U., et al. (2016). Sentinel-2 Sen2Cor: L2A Processor for Users. *Proceedings Living Planet Symposium*, 1-8.
- Masek, J., Claverie, M., Ju, J., Vermote, E., & Justice, C. (2015). A Harmonized Landsat-Sentinel-2 Surface Reflectance product: a resource for Agricultural Monitoring. *AGU Fall Meeting Abstracts*.

- Montgomery, J., Hornbuckle, J., Hume, I., & Vleeshouwer, J. (2015). IrriSAT—Weather based scheduling and benchmarking technology. *Proceedings of the 17th ASA Conference*, 20-24.
- Nguy-Robertson, A.L., Peng, Y., Gitelson, A.A., Arkebauer, T.J., Pimstein, A., Herrmann, I., et al. (2014). Estimating green LAI in four crops: Potential of determining optimal spectral bands for a universal algorithm. *Agricultural and Forest Meteorology*, 192–193, 140-148.
- Park, J., Baik, J., & Choi, M. (2017). Satellite-based crop coefficient and evapotranspiration using surface soil moisture and vegetation indices in Northeast Asia. *Catena*, 156, 305-314.
- Paw U, K.T., Qiu, J., Su, H., Watanabe, T., & Brunet, Y. (1995). Surface renewal analysis: a new method to obtain scalar fluxes. *Agricultural and Forest Meteorology*, 74, 119-137.
- Pearson, R.L., & Miller, L.D. (1972). Remote mapping of standing crop biomass for estimation of the productivity of the shortgrass prairie. *Remote Sensing of Environment*, VIII, 1355.
- Pinty, B., & Verstraete, M. (1992). GEMI: a non-linear index to monitor global vegetation from satellites. *Plant Ecology*, 101, 15-20.
- Qi, J., Chehbouni, A., Huete, A.R., Kerr, Y.H., & Sorooshian, S. (1994). A modified soil adjusted vegetation index. *Remote Sensing of Environment*, 48, 119-126.
- Ray, S.S., & Dadhwal, V.K. (2001). Estimation of crop evapotranspiration of irrigation command area using remote sensing and GIS. *Agricultural Water Management*, 49, 239-249.
- Richardson, A.J., & Wiegand, C. (1977). Distinguishing vegetation from soil background information. *Photogrammetric Engineering and Remote Sensing*, 43, 1541-1552.
- Rosa, R., & Tanny, J. (2015). Surface renewal and eddy covariance measurements of sensible and latent heat fluxes of cotton during two growing seasons. *Biosystems Engineering*, 136, 149-161.
- Rosa, R., Dicken, U., & Tanny, J. (2013). Estimating evapotranspiration from processing tomato using the surface renewal technique. *Biosystems Engineering*, 114, 406-413.
- Rozenstein, O., & Adamowski, J. (2017a). Linking Spaceborne and Ground Observations of Autumn Foliage Senescence in Southern Québec, Canada. *Remote Sensing*, 9, 630.
- Rozenstein, O., & Adamowski, J. (2017b). A review of progress in identifying and characterizing biocrusts using proximal and remote sensing. *International Journal of Applied Earth Observation and Geoinformation*, 57, 245-255.
- Rozenstein, O., Qin, Z., Derimian, Y., & Karnieli, A. (2014). Derivation of Land Surface Temperature for Landsat-8 TIRS Using a Split Window Algorithm. *Sensors*, 14, 5768-5780.
- Senay, G.B., Friedrichs, M., Singh, R.K., & Velpuri, N.M. (2016). Evaluating Landsat 8 evapotranspiration for water use mapping in the Colorado River Basin. *Remote Sensing of Environment*, 185, 171-185.
- Spano, D., Snyder, R.L., Duce, P., & Paw U, K.T. (1997). Surface renewal analysis for sensible heat flux density using structure functions. *Agricultural and Forest Meteorology*, 86, 259-271.
- Tanny, J., Haijun, L., & Cohen, S. (2006). Airflow characteristics, energy balance and eddy covariance measurements in a banana greenhouse. *Agricultural and Forest Meteorology*, 139, 105-118.
- Thenkabail, P.S., Smith, R.B., & De Pauw, E. (2000). Hyperspectral Vegetation Indices and Their Relationships with Agricultural Crop Characteristics. *Remote Sensing of Environment*, 71, 158-182.
- Tucker, C.J. (1979). Red and photographic infrared linear combinations for monitoring vegetation. *Remote Sensing of Environment*, 8, 127-150.
- Viña, A., Gitelson, A.A., Nguy-Robertson, A.L., & Peng, Y. (2011). Comparison of different vegetation indices for the remote assessment of green leaf area index of crops. *Remote Sensing of Environment*, 115, 3468-3478.